A 3D Biohybrid Real-Scale Model of the Brain Cancer Microenvironment for Advanced In Vitro Testing

ADVANCED MATERIALS TECHNOLOGIES
www.advmattechnol.de

A 3D Biohybrid Real-Scale Model of the Brain Cancer Microenvironment for Advanced In Vitro Testing

Omar Tricinci, Daniele De Pasquale,* Attilio Marino,* Matteo Battaglini, Carlotta Pucci, and Gianni Ciofani**

The modeling of the pathological microenvironment of the central nervous system (CNS) represents a disrupting approach for drug screening for advanced therapies against tumors and neuronal disorders. The in vitro investigations of the crossing and diffusion of drugs through the blood–brain barrier (BBB) are still not completely reliable, due to technological limits in the replication of 3D microstructures that can faithfully mimic the in vivo scenario. Here, an innovative 1:1 scale 3D-printed realistic biohybrid model of the brain tumor microenvironment, with both luminal and parenchyma compartments, is presented. The dynamically controllable microfluidic device, fabricated through two-photon lithography, enables the triple co-culture of hCMEC/D3 cells, forming the internal biohybrid endothelium of the capillaries, of astrocytes, and of magnetically-driven spheroids of U87 glioblastoma cells. Tumor spheroids are obtained from culturing glioblastoma cells inside 3D microcages loaded with superparamagnetic iron oxide nanoparticles (SPIONs). The system proves to be capable in hindering dextran diffusion through the bioinspired BBB, while allowing chemotherapy-loaded nanocarriers to cross it. The proper formation of the selective barrier and the good performance of the anti-tumor treatment demonstrate that the proposed device can be successfully exploited as a realistic in vitro model for high-throughput drug screening in CNS diseases.

1. Introduction

According to the World Health Organization, central nervous system (CNS) neoplasms and neurological disorders will affect an increasing number of people worldwide in the next decades. Nowadays, they account for over 6% of the global burden of diseases, with high economic and social costs.[1] Among CNS cancers, glioblastoma (GB) is the most common. In essence, it represents 15% of all intracranial neoplasms and more than 50% of all gliomas, with a poor level of recovery.[2]

The main limitations for therapeutic investigations arise from the extreme complexity of the anatomy of the brain, in particular concerning the blood–brain barrier (BBB).[3–5] The barrier, whose primary function is the protection of the CNS from undesirable substances and pathogens, represents an extremely selective obstacle to almost all drugs that could have a therapeutic effect.[6,7] For this reason, there has been an increasing interest in the study of drug delivery through the BBB into the brain compartment, since it could lead to the elaboration of new advanced therapies against CNS tumors and disorders.[8] In this framework, it is evident how the development of in vitro devices could help in modeling the brain microenvironment and in high-throughput drug screenings.[9] Starting from relatively simple approaches based on artificial membrane permeability assays[10] and transwell assays,[11] research efforts have been moved to the development of 2D[12–18] and 3D[19–28] microfluidic lab-on-a-chip devices that could properly mimic the natural BBB and the relative interaction with drugs.[29,30] However, to date, the technological limits of the available fabrication approaches do not allow reproducing at the natural dimensional scale the brain microcapillaries, that are characterized by a diameter of about 10–20 µm.[5] Furthermore, there are no examples of microfluidic systems that present both a realistic barrier model and an accurate 3D model of the pathological milieu.

In this article, we present the first 1:1 scale 3D-printed realistic microfluidic device for the modeling of the brain tumor microenvironment and of its associated blood neurovasculature, suitable for testing the efficacy of different anticancer therapies in vitro.

In particular, this solution proposes a strong innovation with respect to the platforms already present on the market and in the literature. First of all, the dynamic microfluidic system resembles both the luminal compartment and the parenchyma compartment, where the selected model of the pathological condition can be established. Moreover, it ensures the real-scale

Dr. O. Tricinci, D. De Pasquale, Dr. A. Marino, Dr. M. Battaglini, Dr. C. Pucci, Prof. G. Ciofani
Smart Bio-Interfaces
Istituto Italiano di Tecnologia
Viale Rinaldo Piaggio 34, Pontedera 56025, Italy
E-mail: omar.tricinci@iit.it; danieledepasquale@iit.it; attilio.marino@iit.it; gianni.ciofani@iit.it

The ORCID identification number(s) for the author(s) of this article can be found under https://doi.org/10.1002/admt.202000540.

DOI: 10.1002/admt.202000540

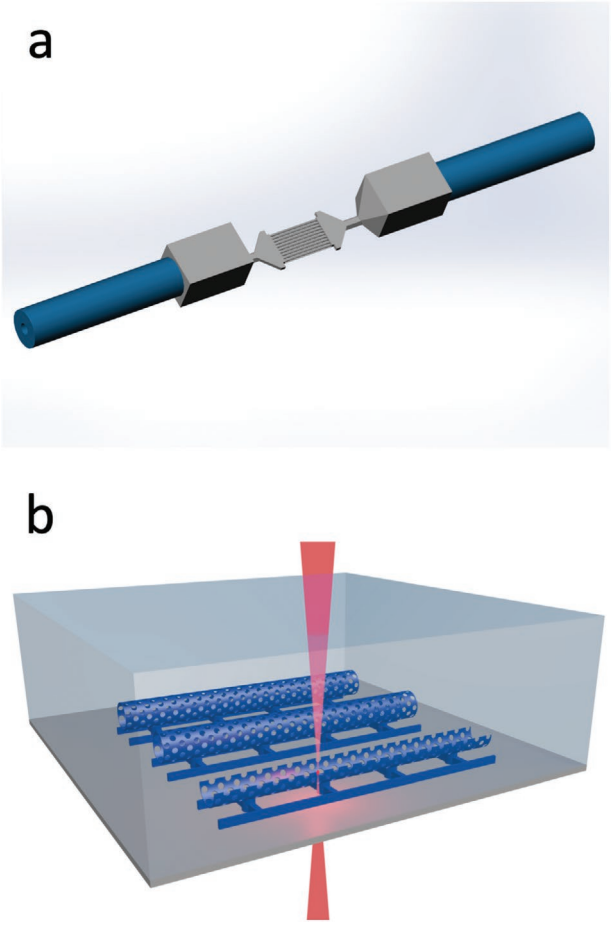

Figure 1. a) 3D depiction of the microfluidic device for the modeling of the brain tumor microenvironment; b) scheme of the TPL fabrication of the microfluidic system mimicking the BBB.

biomimetic model of the pathological microenvironment, considering the complex interactions between different tissues. Finally, this microdevice is equipped with a configurable magnetic-based system that allows to seed cells and to assemble the tumor components of the pathologic scenario.

The microfluidic system is composed of 3D biomimetic brain capillaries fabricated in the shape of an array of aligned porous microtubes (**Figure 1**a). Endothelial cells are cultured in the inner surface of the capillaries in order to spontaneously develop a biohybrid barrier. Micropores prevent the endothelial cells from reaching the external surface of the microtubes but allow drugs and nanoparticles to cross the barrier. In the outer part, astrocytes are cultured in order to strengthen the integrity of the barrier and to promote the same in vivo cell–cell interactions that, for example, are involved in tissue repair and regeneration.[9,18,21,22,31,32] The artificial BBB is connected to a microfluidic pumping system that finely controls the pressure, and thus the flow, of the cell culture medium in the circuit. In this way, it is possible to simulate the physiological parameters to further mimic the in vivo conditions: the flow rate of the medium inside the luminal bio-hybrid microvessels can be imposed to values comparable to those present in vivo in the brain. In fact, the proper flow-induced shear stress on the walls of the artificial barrier represents a fundamental stimulus that cannot be ignored, when envisioning a bioinspired CNS in vitro microenvironment, causing the most insidious poor similarity to the natural counterpart.[13,24] Finally, the possibility of co-culturing various types of cells allows to faithfully reproduce personalized physiological and pathological conditions that can be faced with ad hoc strategies. The presence of magnetically-driven 3D microcages loaded with tumor cells and interacting with the biohybrid interface represents a remarkable innovation in that direction.

Regarding the latter aspect, 3D tumor cultures represent an essential goal when performing anticancer in vitro studies,[33–35] since they can overcome a series of limitations that 2D cultures reveal when shifted into in vivo experiments.[36] In particular, great differences have been demonstrated about drug resistance, tumor aggressiveness, and microenvironment development.[37,38] However, a 3D tumor shape translates into a decrease of diffusion of nutrients and oxygen and, in the anticancer scenario, into a decrease of the rate of penetration of drugs or nanovectors, leading to a reduction of apoptotic effects. Hypoxia is an important aspect for cancer development, since solid tumors with a diameter larger than 200 µm and without blood flow start to express pro-angiogenetic factors and hypoxia-inducible factor (HIF1α) that change the cancer cell phenotype.[39] Different type of strategies exist to obtain 3D tumor models, such as growing cells in low adhesion conditions in order develop cell aggregations in spheroids, or cell culturing in specific supports like inserts or scaffolds.[40–42] In this work, we have combined the properties of the spheroids with the benefits of cage-like scaffolds in trapping cells.[43] We designed and fabricated 3D microcages with appropriate pores and cracks, allowing the passage of nutrients and respiratory gases and ensuring, through cell migration, the proper formation of spheroids of about 200 µm in diameter.

So far, the main obstacle in the production of such type of devices has been the inherent technical limitations of traditional microfabrication techniques that prevent the replication of 3D structures at the microscale. In this work, the microfluidic device and the 3D tumor scaffolds were fabricated by means of two-photon lithography (TPL). This technique allows for the fabrication of complex 3D structures (Figure 1b), with features at the sub-micrometer scale with outstanding results in terms of resolution, reproducibility, and reliability.[26,44,45]

In this article, we tested the effectiveness of the proposed bioinspired microfluidic chip in modeling the GB microenvironment; we verified the formation of a biohybrid BBB and its capability to be permeable to drug-loaded nanoparticles for the treatment of the tumor.

2. Results and Discussion

2.1. Microfluidic Device

The microfluidic chip was designed in order to faithfully emulate the anatomy of the physiological BBB (**Figure 2**a–d). The dimensioning of the various components was calibrated according to microfluidic simulations already investigated in a previous work of ours.[26] The microfluidic component consists of an array of ten microtubes of a length of 1.1 mm. Each capillary, nominally with a diameter of 50 µm and a thickness of 2 µm, is composed of three parts: the two ones at the ends

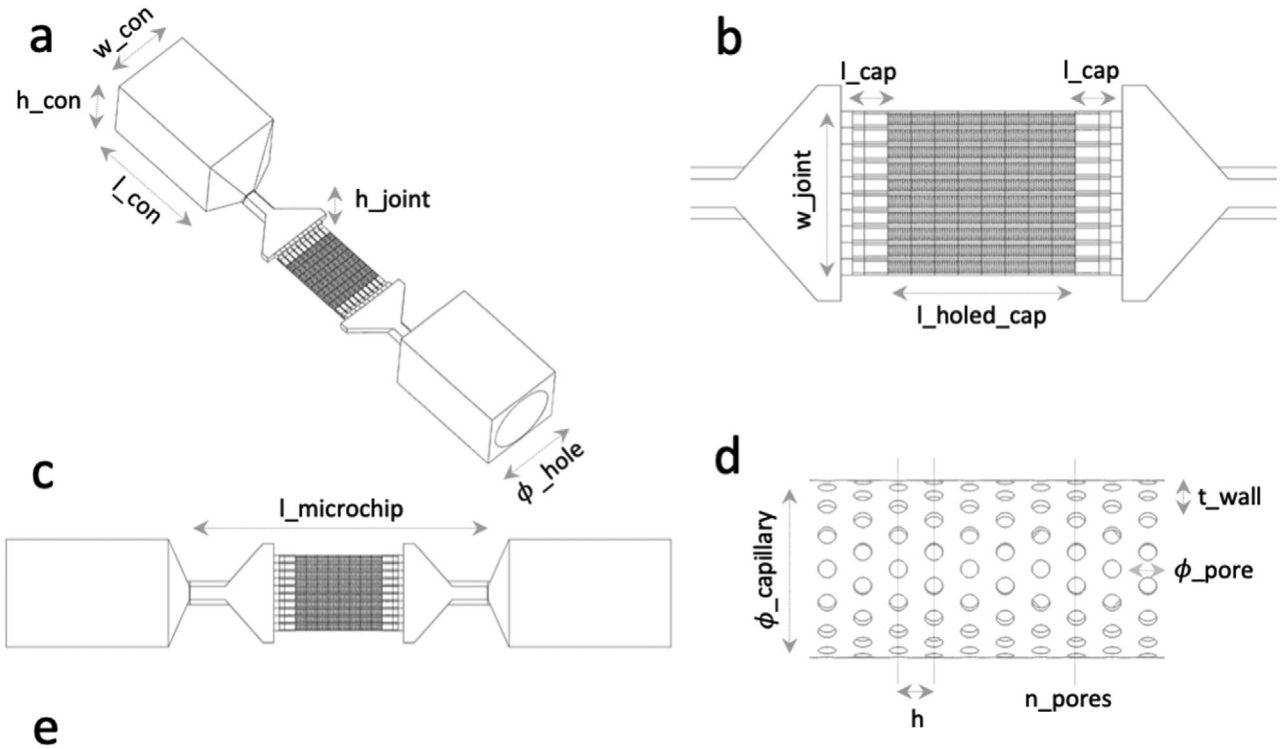

e

l_microchip	l_con	w_con	h_con	h_joint	ϕ_hole	w_joint
2.65 mm	1.7 mm	900 µm	900 µm	80 µm	830 µm	700 µm
l_cap	**l_holed_cap**	**ϕ_capillary**	**t_wall**	**n_pores**	**h**	**ϕ_pore**
150 µm	800 µm	50 µm	2 µm	16	10 µm	5 µm

Figure 2. Views of the microfluidic device: a) perspective view; b) top view of the capillaries array; c) top view of the entire microfluidic device; d) detailed design of the porous microtube; and e) main geometrical parameters of the design.

(150 µm in length) are plain, while the central one (800 µm in length) is porous, with pores of 5 µm in diameter. The purpose of the parts without holes is to ensure the establishment of a laminar flow at the central region that represents the effective biohybrid BBB. The capillaries are linked to a joint on both sides, and then to two connectors that allow the microfluidic device to be linked to a pumping system. The main geometrical parameters of the structure are reported in Figure 2e.

Obtained microfluidic device is depicted in **Figure 3**. Scanning electron microscopy (SEM) images (Figure 3a,c–e) and optical (Hirox) images (Figure 3b) show the outstanding results in terms of resolution of the structures, also confirming the high reproducibility and accuracy of the TPL technique. This aspect is also remarked by the analysis of the pores shown in Figure 3d,e: they have an average diameter of about 4 µm, with a very low dispersion of the data (3.98 ± 0.11 µm). As expected, the pore diameter results to be about 1 µm smaller than the nominal one, since the lateral size of the exposed voxel is about 0.5 µm. Moreover, looking at the surface of the microtubes (Figure 3e), it is possible to appreciate a micro- and nanoroughness due to the slicing parameters of the 3D model and to the vertical size of the exposed voxel, that is about 1 µm. The presence of this morphological feature could represent an advantage in case of biological application, since it ensures a stronger adhesion and growth of cells.[46]

2.2. Biohybrid Barrier Formation

The endothelial cells hCMEC/D3, seeded inside the device through a syringe, resulted to be homogeneously dispersed in the intratubular space (see Video S1, Supporting Information). In **Figure 4**a, the presence of the endothelial cells in the capillaries can be easily detected.

The evaluation of the proper formation of the biohybrid barrier was carried out with three different experiments.

The first qualitative analysis was performed using confocal laser scanning microscope. The results are illustrated in Figure 4b,c: from the section of a part of the capillary and from the 3D reconstruction, it is evident how the endothelial cells were able to reach and settle on the inner surface of the microtubes, after 5 days of culture.

The tightness of the biohybrid BBB was furthermore quantitatively investigated by means of a fluorescently-labeled dextran permeability test. In many models of the BBB, dextran is commonly used since it is able to cross a leaky BBB while being excluded from a healthy one.[30] In Figure 4d, the graph of the extratubular concentration of the fluorescent dextran during time-lapse fluorescence imaging is reported. The concentration in the case of the biohybrid system (with hCMEC/D3 endothelial cells and astrocytes) appears to be much lower with respect to the control without cells, thus proving the effectiveness of

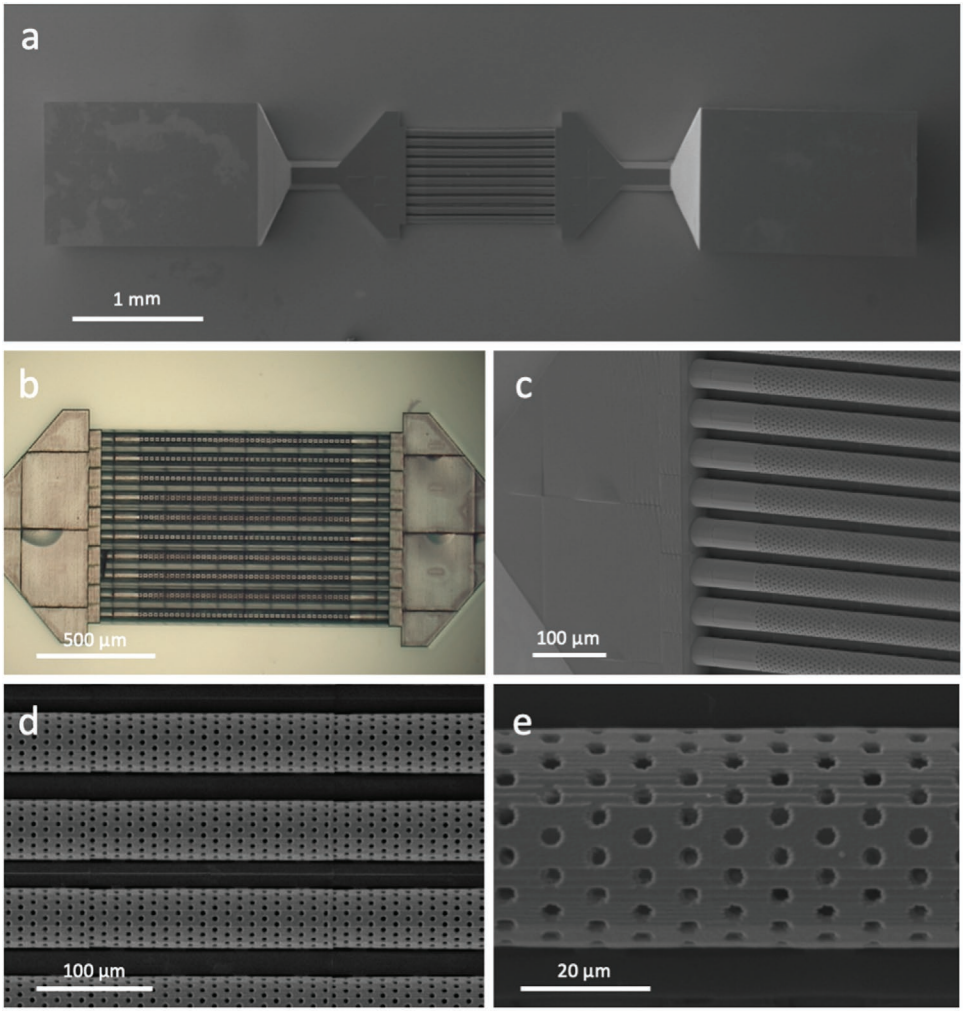

Figure 3. a) SEM image of the top view of the microfluidic device; b) optical image of the capillary array; c) detail of the link between the capillaries and the joint (SEM image); d) detail of the porous microtubes (SEM image); and e) high magnification of a microtube, showing the surface microroughness (SEM image).

formation of the 3D barrier around the inner surface of the microtubes. For example, after 700 s, the concentration of the dextran in the extratubular medium results to be about 3 µg mL^{-1} in the case of cultured endothelial cells, that is lower than the value of about 8 µg mL^{-1} found for the control. The fluorescence values were derived from the average fluorescence intensity in a calibration curve reported in Figure S1, Supporting Information.

In Figure 4e–h, representative images of the fluorescence in the extratubular region are reported for the both experimental conditions: after 700 s, the difference in fluorescence is evident, since most of the dextran was able to permeate and diffuse outside the porous microtubes in the absence of cells with respect to the tight biohybrid barrier (Figure 4f vs h). Several other fluorescence time-lapse frames are reported in Figure S2, Supporting Information.

Finally, we tested the trans-endothelial electrical resistance (TEER) of the biohybrid chip, in particular studying the effects of the cellular components. We found a value of TEER of 56 ± 20 Ω cm^2 for the configuration with endothelial cells hCMEC/D3 inside the microtubes. The presence of human astrocytes induced an increase of the TEER to a value of 75 ± 16 Ω cm^2, showing their effect in promoting the integrity of the barrier.

2.3. Tumor Treatment with Nanocarriers

The treatment of a controlled pathological microenvironment is an indispensable test in order to prove the effectiveness of the proposed platform and to lead to the intensive exploitation of this technology for in vitro drug screening. In particular, the modeling and the treatment of the GB microenvironment was chosen as specific scenario, using antibody-functionalized nutlin-loaded nanostructured lipid carriers (Ab-Nut-NLCs) as anti-tumor agents.

After the verification of the formation of the biohybrid BBB and of its capability to be not permeable to specific molecules, we investigated the permeability to drug-loaded nanoparticles for the treatment of the tumor. This process went through the

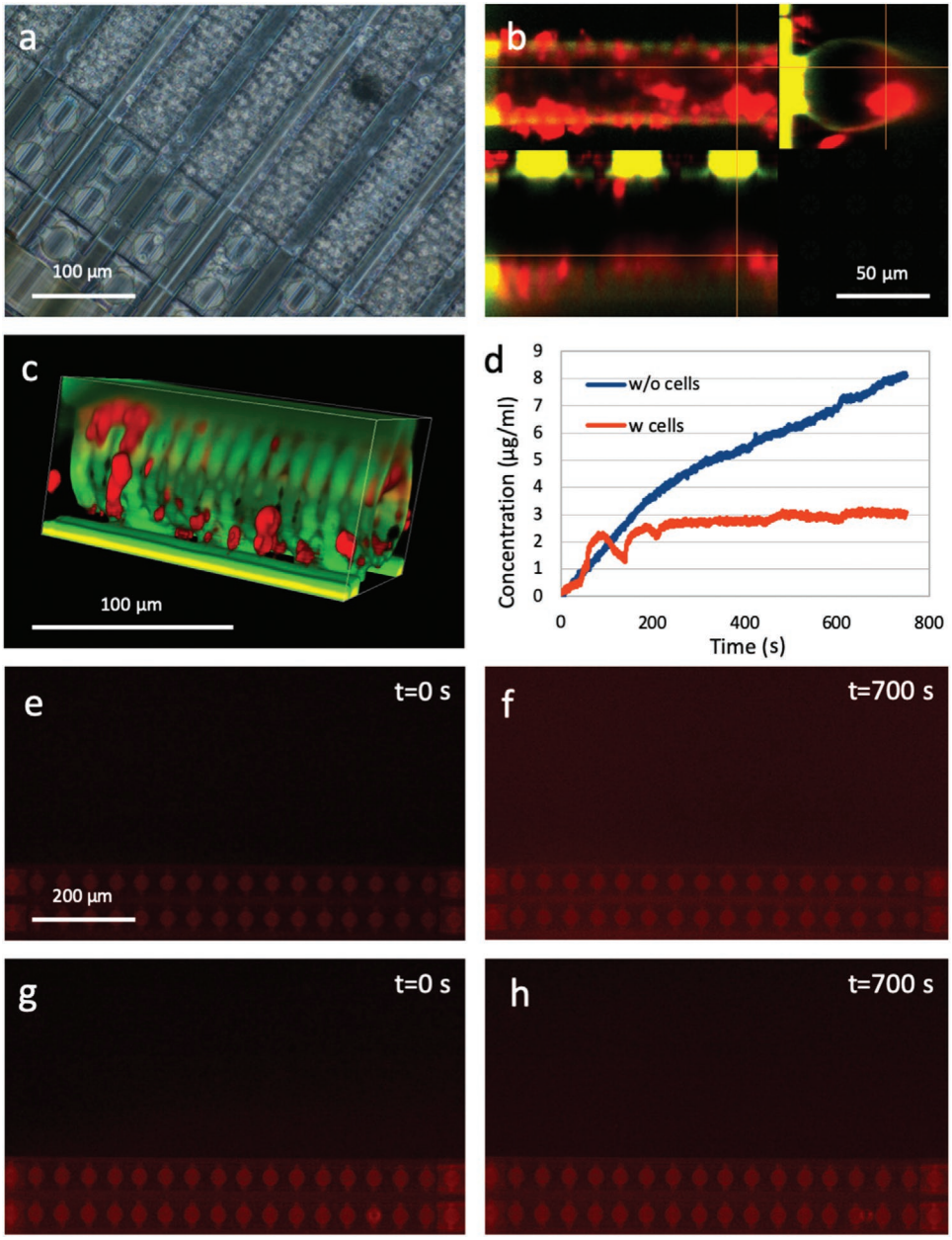

Figure 4. a) Optical image of the endothelial cells seeded inside the capillaries; b) section views of the biohybrid capillary acquired at the confocal microscope: red represents endothelial hCMEC/D3 cells, green represents the microfabricated capillary; c) 3D reconstruction of the biohybrid capillary; d) extratubular concentration graph of the fluorescent dextran monitored during time-lapse fluorescence imaging in the presence and without endothelial hCMEC/D3 cells inside the porous microtubes; fluorescence images of e,f) TRITC-dextran in the extratubular region pumped in the microfluidic system without cells and g,h) in the biohybrid microsystem with hCMEC/D3 cells, acquired at time $t = 0$ and $t = 700$ s.

validation of several steps: the proper seeding of the tumor cells within the microcages, their detachment from the substrate and approach to the microfluidic device, and finally the diffusion of therapeutic nanocarriers through the barrier towards the tumor.

The magnetically-responsive cage-like scaffolds (MRCSs) resulted to be structurally stable despite the high aspect ratio of the geometry, as shown in **Figure 5**a,b. They also demonstrated to be suitable for the seeding of the U87 GB cells: once deposited and cultured in the MRCSs, these procedures led to the development of one spheroid per MRCS after 5 days of growing (Figure 5c).

To further investigate the proliferative phase of the spheroid cell population and its distribution, we performed immunofluorescence analysis against Ki-67 marker, since it is expressed during the interphase of cell cycle and disappears when the cells enter in quiescent phase (G0).[47] As show in Figure S3, Supporting Information, the labeling is mostly distributed in the external layer of the spheroids while the core part is poor of green spots: it means that 3D magnetically-driven scaffolds

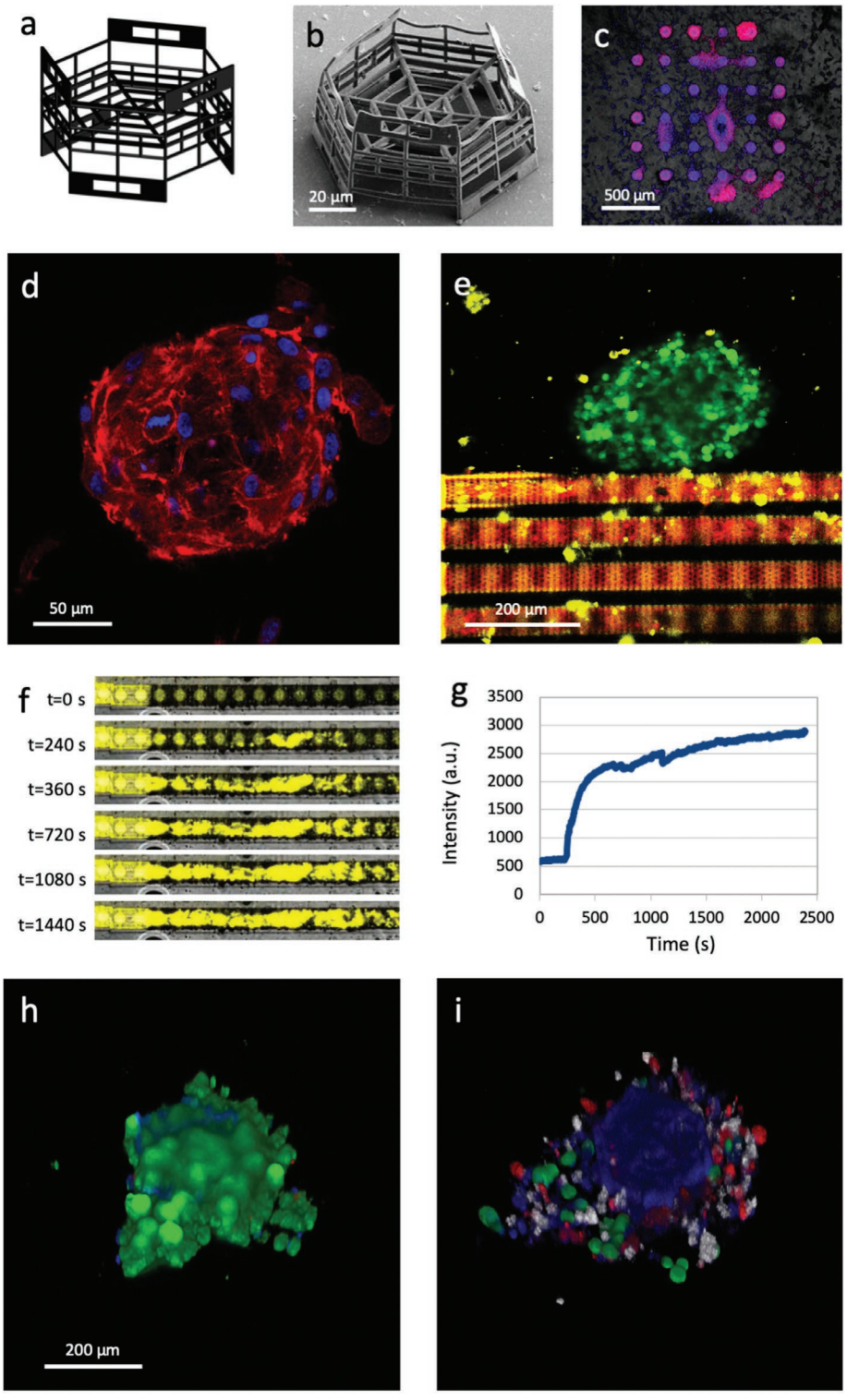

Figure 5. a) 3D rendering of the magnetic microcage; b) SEM image of the fabricated microcage; c) fluorescence image of the array of tumor spheroids before the detachment from the glass substrate; d) confocal microscopy acquisition of a tumor spheroid (U87 cells seeded into the microcage): red represents F-actin, blue represents nuclei; e) confocal microscopy image of the biohybrid GB model: red represents the microtubes with endothelial hCMEC/D3 cells, yellow represents astrocytes, green represents spheroids of U87 GB cells; f) fluorescence time-lapse images of the fluorescent nutlin-loaded nanocarriers dispersion pumped in the selected microtube; g) intratubular fluorescence of nutlin-loaded nanocarriers flow monitored during time-lapse fluorescence imaging, in the presence of endothelial hCMEC/D3 cells inside the porous microtubes and astrocytes outside; h) control spheroid and i) treated tumor spheroid subjected to LIVE/DEAD assay for quantitative analysis of the effect of the antitumor treatment: green represents calcein, red represents EthD-1, blue represents nuclei, and white represents nutlin-loaded nanocarriers.

maintained the typical organization observed in the spheroid grown without any scaffold; in particular, the external layers of cells are in interphase of cell cycle, while the inner part cells are quiescent.[48–50]

The magnetically controllable spheroids were easily removed with a pipette and easily driven with an external magnet close to the BBB model (Figure S4 and Video S2, Supporting Information). In Figure 5d, a confocal microscopy image of the spheroid is reported, showing a dense and compact arrangement of the tumor cells that can provide an in vitro good model of the GB scenario.

Once the dispersion of magnetically-controlled spheroids in culture medium was released on the top of the microfluidic chip, the tumor structures were easily moved in proximity of the artificial barrier. This verified the feasibility to obtain the desired biohybrid system composed of the triple co-culture of endothelial cells hCMEC/D3 inside the microtubes and of astrocytes and U87 cells outside (Figure 5e).

After the magnetic positioning of the tumor spheroids close to the capillaries, a flow of Ab-Nut-NLCs in culture medium was established inside the microtubes. Figure 5f shows the fluorescence time-lapse images of the fluorescent dispersion pumped in the microtubes, with a fluid speed of 1 mm s^{-1} (see also Video S3, Supporting Information). In Figure 5g, the graph of the intratubular fluorescence of the Ab-Nut-NLCs flow, monitored during time-lapse imaging, is shown.

The capability of the Ab-Nut-NLCs to cross the biohybrid BBB and the relative effect of the antitumor treatment was demonstrated by means of a LIVE/DEAD assay on the tumor spheroids. The results of the test for the treated spheroids and the untreated controls are illustrated in Figure 5h,i and Figure S5, Supporting Information. About 70% of the GB cells inside the microcage resulted to be positive for ethidium homodimer-1, thus confirming the effectiveness of the treatment.

3. Conclusions

The investigation of drug delivery through the BBB to the brain is at the center of an intensive research, since it can lead to the development of novel therapies against brain cancer and many neurodegenerative diseases.

Here we fabricated a 3D, real-scale, and bioinspired microfluidic device, by means of TPL, that reproduces, for the first time, a realistic biohybrid model of the GB microenvironment. The proposed biomimetic dynamic system is characterized by microcapillary diameter sizes and fluid flows similar to the in vivo counterpart, thus representing a disruptive innovation with respect to other models currently well-established in biomedicine. Our system resembles both the luminal compartment and the parenchyma compartment, where the appropriate model of the pathological microenvironment has been established. Moreover, it is fabricated as a configurable magnetic-based system that allows to easily perform cell seeding and assembling of the different cellular components. We proved the feasibility of a triple co-culture of hCMEC/D3 cells, forming the internal biohybrid endothelium of the capillaries, astrocytes, and magnetically-driven spheroids of U87 cells. This method represents an unprecedented smart co-culturing system that can be potentially exploited in future prototypes for the development of different multi-cellular platforms for more physiologically relevant scenarios. We demonstrated the efficient development of a biohybrid BBB that showed good performances in terms of TEER and in hindering dextran diffusion; meanwhile, the barrier was permeable to nutlin-loaded nanocarriers that were exploited as a proof of concept of GB cells treatment.

The proposed platform represents a realistic model of the BBB for in vitro high-throughput drug screening for testing novel compounds in the presence of tumors that can be obtained from patient biopsies, thus providing personalized medications. Moreover, this new dual-component system will provide more reliable predictions of the final outcomes with respect to in vivo studies, well discriminating the most promising anticancer strategies already at the in vitro stage. This paradigm can potentially be extended to several pathologies related to the CNS, obtaining experimental results with great reproducibility and biomimicry.

4. Experimental Section

Design and Fabrication: All the components of the proposed device were modeled using the software SolidWorks. The chip was fabricated on a glass substrate by means of a Photonic Professional system (Nanoscribe GmbH), using a negative tone IP-S photoresist (Nanoscribe GmbH). After rinsing the substrate with acetone, isopropyl alcohol (IPA), and deionized water, a drop of IP-S photoresist was cast on it. The objective (25×, NA 0.8) of the instrument was put in immersion in the photoresist that was exposed to a laser beam (Calman laser source) with a center wavelength of 780 nm, using different laser writing parameters for the different components of the system. The capillaries were fabricated with a writing speed of 20 mm s^{-1} and a laser power of 63 mW, the joints with a writing speed of 20 mm s^{-1} and a laser power of 72 mW, while the rest of the device with a writing speed of 100 mm s^{-1} and a laser power of 180 mW (see Video S4, Supporting Information). The sample was then developed for 45 min in propylene glycol methyl ether acetate (PGMEA, Sigma-Aldrich) and rinsed with IPA and deionized water for 10 min in order to ensure the perfect cleaning of the capillaries from the uncured photoresist.

Two polyether ether ketone (PEEK) tubes (1/32″ o.d. × 0.010″ i.d.) of a length of 20 cm were glued at the connectors (Figure S6, Supporting Information) by means of a UV curable resin (AA 3494 Loctite). The system was located and sealed into a 3D printed ring (fabricated in Durable resin by means of Form2, Formlabs) in order to form a transparent box while performing all the experiments under microscope (Figure S7, Supporting Information).

The MRCSs for the tumor cell cultures were designed as hexagonal prisms with six 75 µm-high perimetric cylindrical pillars with a diameter of 2 µm. The inner grids consist of three concentric hexagons having a diagonal length of 120 µm. They were fabricated using a nontoxic negative photoresist, IP-L (Nanoscribe GmbH), loaded with 10 µg mL^{-1} of superparamagnetic iron oxide nanoparticles (SPIONs) of 3 nm in diameter (US Research Nanomaterials, Inc.). The IP-L/SPIONs dispersion was obtained through sonication for 5 min in ice bath with a Bandelin ultrasonic probe (8 W). The structures were obtained by means of the Photonic Professional system with oil objective (63×, NA 1.4), writing speed of 40 mm s^{-1}, and laser power of 144 mW. After the photopolymerization, the samples were developed at room temperature for 30 min with SU-8 Developer (Microchemicals GmbH) and washed for 15 min with IPA and stored in ultrapure water until use. The pre- and post-treatments of the samples were identical to those performed for the microfluidic chip.

Microfluidic Circuit Setup: The assembly of the biohybrid chip went through two phases. At first, the cells had to be seeded into the capillaries for the culture: at this aim, the PEEK tubes linked to the connectors were linked and sealed with the UV curable resin (AA 3494 Loctite) to two syringes. Afterwards, the tubes were cut and connected to the pumping system (Figure S8, Supporting Information), in order to employ the chip in all the subsequent experiments.

The pumping system (Fluigent) is composed of two main components that control the flow and the pressure inside the capillaries, enabling the fine tuning of the microfluidic parameters. A reservoir is connected to a pressure system that makes the liquid flow through a capillary and reach a flowmeter connected in series to the artificial BBB. The biohybrid chip is then connected to a waste reservoir. The flowmeter is linked via software to the pump in a closed loop so that the desired flow is maintained.

This setup was exploited for the dextran diffusion test and for the drug treatment of tumor spheroids.

Cells Seeding, Culture, and Staining: The seeding of endothelial cells inside the capillaries was manually performed by means of a syringe. Human cerebral microvascular endothelial cell line (hCMEC/D3; Merck Millipore) has been adopted since it is largely considered a stable BBB model in CNS drug screening.[51] hCMEC/D3 cells were cultured in T75 flasks in proliferation conditions using EndoGRO-MV (Sigma-Aldrich), supplemented with EndoGRO-MV Supplement kit (5% heat-inactivated FBS, 5% L-glutamine, 0.2% EndoGRO-LS supplement, 5 ng mL^{-1} rhEGF, 1 µg mL^{-1} hydrocortisone hemisuccinate, 0.75 U mL^{-1} heparin sulfate, 50 µg mL^{-1} ascorbic acid; Sigma-Aldrich), and 1% penicillin-streptomycin (100 IU mL^{-1} of penicillin and 100 µg mL^{-1} of streptomycin; Gibco). hCMEC/D3 cells were seeded at full confluence (30 000 cells cm^{-2}) inside the 3D porous microtubes. Human primary astrocytes (Innoprot) were cultured in proliferation conditions using DMEM high glucose (Sigma-Aldrich), supplemented with 5% heat-inactivated FBS (Gibco), 3% astrocyte growth supplement (Sigma-Aldrich), 1% L-glutamine (stock 200×10^{-3} M; Gibco), 1% sodium pyruvate (stock 100×10^{-3} M; Gibco), and 1% penicillin-streptomycin (100 IU mL^{-1} of penicillin and 100 µg mL^{-1} of streptomycin; Gibco). To visualize hCMEC/D3 inside the porous tubes, cells were fixed and the cytoskeleton stained with TRITC-phalloidin (Sigma-Aldrich); nuclei were counterstained with Hoechst (Invitrogen). Cells were incubated for 40 min with 10% goat serum (Sigma-Aldrich) in DPBS (Sigma-Aldrich) and subsequently with a solution of 10% goat serum-containing 2.5 µg mL^{-1} of TRITC-phalloidin (Sigma-Aldrich) and 5 µg mL^{-1} of Hoechst (Invitrogen) for 1 h; after the incubation, cells were washed twice in DPBS (Sigma-Aldrich) and then imaged at the confocal laser scanning microscope (C2s system, Nikon) with a 60× oil immersion objective. To improve the BBB properties of the device, after 5 days from the seeding of hCMEC/D3 cells inside the microporous tubes, human primary astrocytes were seeded on the outside part of the tubes at a cellular density of 10 000 cells cm^{-2}.

Both normal U87 cells (ATCC) and GFP-expressing U87 (Cellomix) were used in this work. The former were employed in the experiments with nanocarriers, the latter were used in the imaging experiments. Both cells lines were cultured in proliferation conditions using high-glucose DMEM (Sigma-Aldrich), supplemented with 10% heat-inactivated FBS (Gibco), 1% L-glutamine (stock 200×10^{-3} M; Gibco), 1% sodium pyruvate (stock 100×10^{-3} M; Gibco), and 1% penicillin-streptomycin (100 IU mL^{-1} of penicillin and 100 µg mL^{-1} of streptomycin; Gibco). For splitting and cell detachment procedures, the cell culture medium was removed, cells were washed with DPBS (Sigma-Aldrich), and incubated for 5 min with trypsin (Sigma-Aldrich). GFP-expressing U87, employed in imaging experiments, were washed thrice with PBS, Ca^{2+} and Mg^{2+} free, treated for 5 min with 0.05% trypsin-EDTA, centrifuged, and re-suspended in DMEM high-glucose complete medium, 5 days before performing experiments. 2×10^4 cells in 30 µL of the cells suspension were seeded in the MRCSs. After 5 days of cell growth in the MRCSs, the constructs were detached from the substrate through suction with a pipette tip and collected for the BBB experiments.

For imaging experiments, both hCMEC/D3 and human primary astrocytes were stained before seeding; briefly, cells were detached and resuspended in 500 µL of complete media supplemented with lipophilic dyes (5×10^{-6} M of DiD for human astrocytes and 5×10^{-6} M of DiI for hCMEC/D3; Thermo Fisher Scientific) and left at 37 °C for 30 min. After the incubation, cells were washed twice through centrifugation and seeded as previously described.

Immunostaining against Ki-67: The spheroids were fixed with 4% paraformaldehyde for 20 min, and after 30 min of incubation with the blocking solution (Triton 100 × 1:1000, 10% goat serum in PBS), they were incubated for 3 h with primary anti-Ki-67 antibody (1:150 dilution; Millipore) at 37 °C. The secondary FITC-conjugated goat anti-rabbit antibody (1:250 dilution; Millipore) was administered for 2 h and, after the washing steps, staining with TRITC-phalloidin (1:200 dilution; Sigma-Aldrich) and Hoechst 33342 (1:1000 dilution; Invitrogen) in PBS was carried out for 1 h at 37 °C. Images were acquired with a C2s confocal microscope (Nikon).

Dextran Diffusion Test: The investigation of the BBB permeability was performed by studying the dextran diffusion through the porous microtubes of the device, both in the absence and in the presence of endothelial hCMEC/D3 cells and astrocytes. A solution of 40 µg mL^{-1} of fluorescent dextran (Dextran, Alexa Fluor 647, MW 10 000 Da; Thermo Fisher) in phenol red-free cell culture medium was used for the test. By means of the micropumping system, the solution was pumped into the device, reaching a flow rate of 1.2 µL min^{-1} in order to ensure a fluid speed of 1 mm s^{-1} inside each of the ten capillaries. This value corresponds to the natural counterpart.[52]

Time-lapse fluorescent imaging was performed for monitoring the concentration of the fluorescent dextran in the extratubular region on one side of the device. Imaging was performed using an epifluorescence microscope (Eclipse Ti, Nikon). The actual concentration was extrapolated from the average fluorescence intensity by means of a calibration curve.

TEER Measurements: TEER measurements were performed in the presence of endothelial cells hCMEC/D3 and also after seeding both endothelial cells and human astrocytes inside the porous capillaries. Before the experiments, two drops of 100 µL phenol red-free DMEM were deposited on the outflow and in the extratubular regions. The measurements were obtained by subtracting the basal values of the microfluidic chip without cells and multiplying the results for the total porous area.

TEER was measured by means of a commercial system (Millipore, Millicell ERS-2 Voltohmmeter) with one electrode positioned in the outflow liquid and the other positioned in the extratubular fluid, in proximity of the porous region.

Nanocarriers Synthesis: Nanostructured lipid carriers loaded with nutlin-3a (Nut-NLCs) were synthetized following a hot sonication protocol (Figure S9, Supporting Information). A lipid mixture composed of 25 mg of 1-stearoyl-*rac*-glycerol (Sigma-Aldrich), 2.5 mg of oleic acid (Sigma-Aldrich), 2.5 mg of 1,2-dipalmitoyl-*rac*-glycero-3-phosphocholine (Sigma-Aldrich), 2 mg of 1,2-distearoyl-*sn*-glycero-3-phosphoethanolamine-*N*-[amino(polyethylene glycol)-2000] (mPEG-DSPE, 5 kDa; Nanocs, Inc.), and 2 mg of biotin-PEG-DSPE (Sigma-Aldrich) was heated at 70 °C (melting temperature of the lipids) together with 1 mg of nutlin-3a (Sigma-Aldrich). A total of 3 mL of pre-heated (70 °C) 1.0 wt% Tween 80 (Sigma-Aldrich) aqueous solution (1.0 wt%) was added to the lipid mixture. The dispersion was then homogenized with an ultrasonic tip for 20 min (amplitude 90%, Fisherbrand Q125 Sonicator), and let to cool down at 4 °C for 30 min. Nut-NLCs were subsequently purified by three centrifugation steps using Amicon centrifuge filters (Ultra-4 Centrifugal Filter Unit, MWCO 100 kDa; Sigma-Aldrich) at 5000 × *g* for 40 min at 4 °C and finally re-dispersed in 1 mL of Milli-Q water (Millipore).

Nut-NLCs were subsequently functionalized with the anti-transferrin receptor antibody (anti-TfR Ab) similarly as previously described.[53] A total of 30 µL of streptavidin-Ab against TfR (0.5 mg mL^{-1}; Abcore) were added to 100 µL of a 5 mg mL^{-1} Nut-NLC dispersion to let the streptavidin interact with the biotin-PEG-DSPE. The functionalized nanocarriers (Ab-Nut-NLCs) were purified by dialysis (molecular weight cut-off of 300 kDa; Spectrum Laboratories, Inc.).

The hydrodynamic size and the ζ-potential of the nanocarriers were evaluated by dynamic light scattering measurements using a Zetasizer Nano ZS90 (Malvern Instruments Ltd.). Analyses were performed at 37 °C on dispersions at a concentration of 100 μg mL^{-1} in ultrapure water. The resulting Ab-Nut-NLCs have an average hydrodynamic diameter of 201.0 ± 4.8 nm, a polydisperisty index (PDI) of 0.132 ± 0.040, and a ζ-potential of –46.7 ± 2.6 mV (Figure S9a,b, Supporting Information). The intensity distribution as a function of the diameter shows a monomodal size distribution.

The morphology and size of Ab-Nut-NLCs was evaluated with transmission electron microscopy (TEM) using a JEOL JEM-1011 (JEOL, Tokyo, Japan) operated at 100 kV on a single-tilt sample holder (Figure S9c, Supporting Information). A drop of the nanocarriers, previously sonicated for 2 min, was deposited on a Cu grid (150 mesh) coated with an ultrathin amorphous carbon film, let there for 20 s, and removed with filter paper. The grid was rinsed with Milli-Q water. The contrast of the Ab-Nut-NLCs was enhanced by depositing a drop of uranyl acetate 1% in water for 60 s. This solution was then removed with filter paper.

The amount of nutlin-3a loaded into the nanocarriers was quantified by high-performance liquid chromatography (HPLC) with a Shimadzu LC-20AT, using a C-18 column (150 mm × 4.6 mm i.d., 5 μm particle size). Briefly, 1 mg of freeze-dried Ab-Nut-NLCs were dissolved in 400 μL of methanol and heated at 70 °C for 1 h. Later, 100 μL of cold ultrapure water was added and the dispersion was centrifuged for 90 min at 4 °C at 16 000 × *g*. The supernatant was collected and injected into the HPLC column, with a mobile phase composed of methanol/water (80/20), pumped in isocratic mode at a flow rate of 1 mg mL^{-1}. Nutlin-3a peak was expected at a retention time of 4.77 min and its intensity at 260 nm measured with an UV detector. The drug loading (%), expressed as (encapsulated drug mass/total mass of the nanocarriers) × 100, was found to be 0.8% ± 0.1% wt.

For the fluorescence imaging of nanocarriers, 100 μL of 5 mg mL^{-1} Ab-Nut-NLCs were labeled with 5 μL of Vybrant DiD (1,1′-dioctadecyl-3,3,3′,3′-tetramethylindocarbocyanine perchlorate; Thermo Fisher).

Tumor Treatment Setup: After 6 days of incubation, the biohybrid device with the developed BBB was connected to the pumping system filled in the reservoir with a dispersion of 400 μg mL^{-1} Ab-Nut-NLCs in culture medium. The tumor spheroids, composed of U87 cells seeded into the microcages, were dispersed on the top of the central region of the device and were located in proximity of the capillaries array using an external magnet (size 40 × 10 × 10 mm, Br = 1.31 ± 0.02 T, grade N42). The fluid flow in the microfluidic device was set to a value of 4.7 mL min^{-1}, like in natural conditions, and was constantly regulated by the pumping system.

The fluorescence of the Ab-Nut-NLCs flowing inside the capillary was acquired in time-lapse fluorescent imaging through epifluorescence microscope (Eclipse Ti). Finally, the values of fluorescence were converted into the values of concentration by means of a calibration curve.

Cell Viability Test: Cell viability tests were performed in order to investigate the effectiveness of Ab-Nut-NLCs. The tests were performed on treated spheroids and on controls after 24 h from the flow experiment. Both samples were stained with LIVE/DEAD Viability/Cytotoxicity Kit (Invitrogen); briefly, cells were incubated with complete medium supplemented with 4 × 10^{-6} M EthD-1, 2 × 10^{-6} M calcein AM, and 5 μg mL^{-1} Hoechst (Invitrogen) for 30 min at 37 °C, washed twice with complete medium, and then imaged through confocal laser scanning microscopy (C2s system). The cell mortality was reported as the percentage of cells positive for ethidium homodimer-1.

Supporting Information

Supporting Information is available from the Wiley Online Library or from the author.

Acknowledgements

O.T. and D.D.P. contributed equally to this work. This work was funded by the European Research Council (ERC) under the European Union's Horizon 2020 research and innovation program (grant agreement N°832045, BBBhybrid). The authors would like to thank Dr. Simone Lauciello (Istituto Italiano di Tecnologia, Genova, Italy) for the transmission electron microscopy imaging.

Conflict of Interest

D.D.P., A.M., and G.C. declare a patent filing related to some of the technologies presented in this article (Italian patent application IT102019000018614, October 11, 2019). The authors declare no other conflict of interest.

Keywords

biohybrid microfluidic systems, biomimetics, blood–brain barrier, glioblastoma, two-photon lithography

Received: June 4, 2020
Revised: July 29, 2020
Published online: August 23, 2020

[1] World Health Organization, *Neurological Disorders: Public Health Challenges*, World Health Organization, Geneva, Switzerland **2006**.
[2] M. D. Johnson, J. B. Atkinson, in *Modern Surgical Pathology*, 2nd ed. (Eds: N. Weidner, R. J. Cote, S. Suster, L. M. Weiss), W. B. Saunders, Philadelphia, PA **2009**, pp. 1984–2038.
[3] N. J. Abbott, L. Rönnbäck, E. Hansson, *Nat. Rev. Neurosci.* **2006**, *7*, 41.
[4] J. D. Huber, R. D. Egleton, T. P. Davis, *Trends Neurosci.* **2001**, *24*, 719.
[5] A. Wong, M. Ye, A. Levy, J. Rothstein, D. Bergles, P. C. Searson, *Front. Neuroeng.* **2013**, *6*, 7.
[6] C. Fang, K. Wang, Z. R. Stephen, Q. Mu, F. M. Kievit, D. T. Chiu, O. W. Press, M. Zhang, *ACS Appl. Mater. Interfaces* **2015**, *7*, 6674.
[7] A. S. Kesselheim, T. J. Hwang, J. M. Franklin, *Nat. Rev. Drug Discovery* **2015**, *14*, 815.
[8] B. Sharma, K. Luhach, G. T. Kulkarni, in *Brain Targeted Drug Delivery System* (Eds: H. Gao, X. Gao), Academic Press, Cambridge, MA **2019**, pp. 53–101.
[9] R. Booth, H. Kim, *Lab Chip* **2012**, *12*, 1784.
[10] L. Di, E. H. Kerns, K. Fan, O. J. McConnell, G. T. Carter, *Eur. J. Med. Chem.* **2003**, *38*, 223.
[11] C. Weidenfeller, C. N. Svendsen, E. V. Shusta, *J. Neurochem.* **2007**, *101*, 555.
[12] J. H. Yeon, D. Na, K. Choi, S.-W. Ryu, C. Choi, J.-K. Park, *Biomed. Microdevices* **2012**, *14*, 1141.
[13] L. M. Griep, F. Wolbers, B. de Wagenaar, P. M. ter Braak, B. B. Weksler, I. A. Romero, P. O. Couraud, I. Vermes, A. D. van der Meer, A. van den Berg, *Biomed. Microdevices* **2013**, *15*, 145.
[14] A. K. H. Achyuta, A. J. Conway, R. B. Crouse, E. C. Bannister, R. N. Lee, C. P. Katnik, A. A. Behensky, J. Cuevas, S. S. Sundaram, *Lab Chip* **2013**, *13*, 542.
[15] B. Prabhakarpandian, M.-C. Shen, J. B. Nichols, I. R. Mills, M. Sidoryk-Wegrzynowicz, M. Aschner, K. Pant, *Lab Chip* **2013**, *13*, 1093.
[16] K. L. Sellgren, B. T. Hawkins, S. Grego, *Biomicrofluidics* **2015**, *9*, 061102.
[17] F. R. Walter, S. Valkai, A. Kincses, A. Petneházi, T. Czeller, S. Veszelka, P. Ormos, M. A. Deli, A. Dér, *Sens. Actuators, B* **2016**, *222*, 1209.
[18] Y. I. Wang, H. E. Abaci, M. L. Shuler, *Biotechnol. Bioeng.* **2017**, *114*, 184.

[19] J. A. Kim, H. N. Kim, S.-K. Im, S. Chung, J. Y. Kang, N. Choi, *Biomicrofluidics* **2015**, *9*, 024115.
[20] J. A. Brown, V. Pensabene, D. A. Markov, V. Allwardt, M. D. Neely, M. Shi, C. M. Britt, O. S. Hoilett, Q. Yang, B. M. Brewer, P. C. Samson, L. J. McCawley, J. M. May, D. J. Webb, D. Li, A. B. Bowman, R. S. Reiserer, J. P. Wikswo, *Biomicrofluidics* **2015**, *9*, 054124.
[21] A. Herland, A. D. van der Meer, E. A. FitzGerald, T.-E. Park, J. J. F. Sleeboom, D. E. Ingber, *PLoS One* **2016**, *11*, e0150360.
[22] H. Xu, Z. Li, Y. Yu, S. Sizdahkhani, W. S. Ho, F. Yin, L. Wang, G. Zhu, M. Zhang, L. Jiang, Z. Zhuang, J. Qin, *Sci. Rep.* **2016**, *6*, 36670.
[23] T. B. Terrell-Hall, A. G. Ammer, J. I. G. Griffith, P. R. Lockman, *Fluids Barriers CNS* **2017**, *14*, 3.
[24] P. P. Partyka, G. A. Godsey, J. R. Galie, M. C. Kosciuk, N. K. Acharya, R. G. Nagele, P. A. Galie, *Biomaterials* **2017**, *115*, 30.
[25] S. Bang, S.-R. Lee, J. Ko, K. Son, D. Tahk, J. Ahn, C. Im, N. L. Jeon, *Sci. Rep.* **2017**, *7*, 8083.
[26] A. Marino, O. Tricinci, M. Battaglini, C. Filippeschi, V. Mattoli, E. Sinibaldi, G. Ciofani, *Small* **2018**, *14*, 1702959.
[27] N. R. Wevers, D. G. Kasi, T. Gray, K. J. Wilschut, B. Smith, R. van Vught, F. Shimizu, Y. Sano, T. Kanda, G. Marsh, S. J. Trietsch, P. Vulto, H. L. Lanz, B. Obermeier, *Fluids Barriers CNS* **2018**, *15*, 23.
[28] B. M. Maoz, A. Herland, E. A. FitzGerald, T. Grevesse, C. Vidoudez, A. R. Pacheco, S. P. Sheehy, T.-E. Park, S. Dauth, R. Mannix, N. Budnik, K. Shores, A. Cho, J. C. Nawroth, D. Segrè, B. Budnik, D. E. Ingber, K. K. Parker, *Nat. Biotechnol.* **2018**, *36*, 865.
[29] M. A. Kaisar, R. K. Sajja, S. Prasad, V. V. Abhyankar, T. Liles, L. Cucullo, *Expert Opin. Drug Discovery* **2017**, *12*, 89.
[30] A. Oddo, B. Peng, Z. Tong, Y. Wei, W. Y. Tong, H. Thissen, N. H. Voelcker, *Trends Biotechnol.* **2019**, *37*, 1295.
[31] G. Adriani, D. Ma, A. Pavesi, R. D. Kamm, E. L. K. Goh, *Lab Chip* **2017**, *17*, 448.
[32] S. P. Deosarkar, B. Prabhakarpandian, B. Wang, J. B. Sheffield, B. Krynska, M. F. Kiani, *PLoS One* **2015**, *10*, e0142725.
[33] M. J. Bissell, D. Radisky, *Nat. Rev. Cancer* **2001**, *1*, 46.
[34] J. Debnath, J. S. Brugge, *Nat. Rev. Cancer* **2005**, *5*, 675.
[35] R. M. Sutherland, B. Sordat, J. Bamat, H. Gabbert, B. Bourrat, W. Mueller-Klieser, *Cancer Res.* **1986**, *46*, 5320.
[36] M. Kapałczyńska, T. Kolenda, W. Przybyła, M. Zajączkowska, A. Teresiak, V. Filas, M. Ibbs, R. Bliźniak, Ł. Łuczewski, K. Lamperska, *Arch. Med. Sci.* **2018**, *14*, 910.
[37] D. Hanahan, R. A. Weinberg, *Cell* **2000**, *100*, 57.
[38] A. L. Harris, *Nat. Rev. Cancer* **2002**, *2*, 38.
[39] T. P. Calmels, V. Mattot, N. Wernert, B. Vandenbunder, D. Stéhelin, *Biol. Cell* **1995**, *84*, 53.
[40] L. Mohammad-Hadi, A. J. MacRobert, M. Loizidou, E. Yaghini, *Nanoscale* **2018**, *10*, 1570.
[41] C. Fischbach, R. Chen, T. Matsumoto, T. Schmelzle, J. S. Brugge, P. J. Polverini, D. J. Mooney, *Nat. Methods* **2007**, *4*, 855.
[42] S. J. Florczyk, K. Wang, S. Jana, D. L. Wood, S. K. Sytsma, J. G. Sham, F. M. Kievit, M. Zhang, *Biomaterials* **2013**, *34*, 10143.
[43] B. Spagnolo, V. Brunetti, G. Leménager, E. De Luca, L. Sileo, T. Pellegrino, P. Paolo Pompa, M. De Vittorio, F. Pisanello, *Sci. Rep.* **2015**, *5*, 10531.
[44] A. Accardo, M.-C. Blatché, R. Courson, I. Loubinoux, C. Thibault, L. Malaquin, C. Vieu, *Small* **2017**, *13*, 1700621.
[45] J.-F. Xing, M.-L. Zheng, X.-M. Duan, *Chem. Soc. Rev.* **2015**, *44*, 5031.
[46] M. Lampin, R. Warocquier-Clérout, C. Legris, M. Degrange, M. F. Sigot-Luizard, *J. Biomed. Mater. Res.* **1997**, *36*, 99.
[47] J. Gerdes, H. Lemke, H. Baisch, H. H. Wacker, U. Schwab, H. Stein, *J. Immunol.* **1984**, *133*, 1710.
[48] J. Laurent, C. Frongia, M. Cazales, O. Mondesert, B. Ducommun, V. Lobjois, *BMC Cancer* **2013**, *13*, 73.
[49] M. Zanoni, F. Piccinini, C. Arienti, A. Zamagni, S. Santi, R. Polico, A. Bevilacqua, A. Tesei, *Sci. Rep.* **2016**, *6*, 19103.
[50] P. M. Aponte, A. Caicedo, *Stem Cells Int.* **2017**, *2017*, 5619472.
[51] B. Weksler, I. A. Romero, P.-O. Couraud, *Fluids Barriers CNS* **2013**, *10*, 16.
[52] A. G. Hudetz, *Microcirculation* **1997**, *4*, 233.
[53] A. Marino, A. Camponovo, A. Degl'Innocenti, M. Bartolucci, C. Tapeinos, C. Martinelli, D. D. Pasquale, F. Santoro, V. Mollo, S. Arai, M. Suzuki, Y. Harada, A. Petretto, G. Ciofani, *Nanoscale* **2019**, *11*, 21227.